# Exometabolomic analysis of decidualizing human endometrial stromal and perivascular cells

Sarah Harden [1,2,3*], Jieliang Zhou [4*], Maria Diniz-da-Costa [1,6], Emma S. Lucas[1], Liang Cui[2],

Keisuke Murakami[5], Jinling Fang[2], Qingfeng Chen[3], Jan J Brosens[1,6], Yie Hou Lee[2,4,7]

[1]Division of Reproductive Health, Clinical Science Research Laboratories, Warwick Medical

School, University of Warwick, Coventry CV4 7AL, UK;

[2]Singapore-MIT Alliance for Research and Technology, Singapore;

[3]Institute of Molecular and Cellular Biology, Agency for Science, Technology and Research,

Singapore;

[4]Translational 'Omics and Biomarkers Group KK Research Centre, KK Women's and Children's

Hospital, Singapore;

[5]Department of Obstetrics and Gynaecology, Juntendo University Faculty of Medicine, Tokyo,

113-8421, Japan;

[6]Tommy's National Centre for Miscarriage Research, University Hospitals Coventry &

Warwickshire, Coventry CV2 2DX, UK;

[7]Obstetrics and Gynaecology Academic Clinical Programme, Duke-NUS Medical School,

Singapore.

**Corresponding author**: Dr. Yie Hou Lee,  Email: yiehou.lee@smart.mit.edu Tel: 65-6238 4013

*These authors contributed equally.

**Abbreviations**: ADA, adenosine deaminase; ADK, adenosine kinase; AICAR, 5-

aminoimidazole-4-carboxamide ribonucleotide; DSC, decidual stromal cell; EnSC, endometrial

stromal cell; FC, fold-change; HPRT, hypoxanthine-guanine phosphoribosyl-transferase; IDO,

indoleamine 2,3-dioxygenase ; IGFBP1, insulin-like growth factor binding portein-1; IMP, inosine monophosphate; MACS, magnetic activated cell sorting; MICA, MHC class I polypeptide-related sequence A; MPA, medroxyprogesterone acetate; MRM, multiple reaction monitoring; NKG2D, killer group 2D receptor (NKG2D); P2R, purinergic receptors; PGE2, prostaglandin E2; PNP, purine nucleoside phosphorylase; PRL, prolactin; PVC, perivascular cells; ROS, reactive oxygen species; SUSD2, sushi domain containing 2; uNK, uterine natural killer cells;  XDH /XOR, xanthine dehydrogenase / xanthine oxidoreductase

## ABSTRACT

Differentiation of endometrial fibroblasts into specialized decidual cells controls embryo implantation and transforms the cycling endometrium into a semi-permanent, immune-protective matrix that accommodates the placenta throughout pregnancy. This process starts during the midluteal phase of the menstrual cycle with decidual transformation of perivascular cells (PVC) surrounding the terminal spiral arterioles and endometrial stromal cells (EnSC) underlying the luminal epithelium. Decidualization involves extensive cellular reprogramming and acquisition of a secretory phenotype, essential for coordinated placental trophoblast invasion. Secreted metabolites are an emerging class of signalling molecules. Here, we used liquid chromatography-mass spectrometry to characterise the dynamic changes in metabolite secretion (exometabolome) of primary PVC and EnSC decidualized over 8 days. We identified 79 annotated metabolites differentially secreted upon decidualization, including prostaglandin, sphingolipid, and hyaluronic acid metabolites. Secreted metabolites encompassed 21 metabolic pathways, most prominently glycerolipid and pyrimidine metabolism. Although temporal exometabolome changes were comparable between decidualizing PVC and EnSC, 32 metabolites were differentially secreted across the decidualization time-course. Further, targeted metabolomics demonstrated a conspicuous difference in xanthine secretion between decidualized PVC and EnSC. Taken together, our findings indicate that the metabolic footprints generated by different decidual subpopulations encode spatiotemporal information that may be important for optimal embryo implantation.

**Keywords**: Endometrium, decidualization, exometabolome, metabolism, perivascular cells.

## INTRODUCTION

Cyclical decidualization, i.e. differentiation of endometrial fibroblasts into specialized decidual cells, is a hallmark of menstruating mammals. [1,2] Rather than being triggered by an implanting embryo, decidualization in menstruating species is initiated during the midluteal phase of each cycle in response to sustained progesterone signaling and rising intracellular cyclic adenosine monophosphate (cAMP) levels. [3] Initially, decidual changes are most prominent in sushi domain-containing 2-positive (SUSD2$^+$) cells surrounding the terminal spiral arterioles and in SUSD2$^-$ stromal cells underlying the luminal epithelium, [4] and then spread to encompass the entire stromal compartment. [3] In parallel, proliferating innate immune cells accumulate foremost uterine natural killer cells. [5] Upon embryo implantation, decidualizing cells rapidly encapsulate the conceptus, [6,7] engage in embryo biosensing and selection, [8,9] and then form an immune-privileged decidual matrix that controls interstitial and intravascular trophoblast invasion. [3,10,11]

Recent studies have shown that decidualization is a multistep differentiation process, which starts with an evolutionarily conserved acute cellular stress response, [12,13] characterized by a burst of reactive oxygen species (ROS) production and release of proinflammatory cytokines. [5,14−16] After a lag period of several days, differentiating cells lose their fibroblastic appearance and emerge as secretory decidual cells with abundant cytoplasm and prominent endoplasmic reticulum. [3] At a molecular level, the decidual transformation of endometrial fibroblasts involves genome-wide remodeling of the chromatin landscape, [17] extensive reprogramming of multiple signal transduction and metabolic pathways, [18−20] and activation of decidual gene networks. [21−23] At a functional level, decidualization transforms endometrial fibroblasts into secretory cells that are anti-inflammatory, [15,24] resistant to stress signals, [15,18,25] and highly responsive to embryonic cues. [8,26]

4

The decidual secretome is highly dynamic. Its composition changes across the different phases of the decidual pathway, [15,16,27] and the amplitude of the secretory response depends on the topography of cells in the native tissue. [4] For example, analysis of paired SUSD2⁻ and SUSD2⁺ cell cultures demonstrated that perivascular SUSD2⁺ cells secrete significantly higher levels of various chemokines and cytokines, including chemokine (C-C motif) ligand 7 (CCL7) and leukemia inhibitory factor (LIF). [4] These observations indicate that topographical microenvironments and chemokine gradients are established upon decidualization, which likely promote and direct trophoblast migration towards the spiral arterioles. Initially, invasion of the vessels results in plugging of these arteries by trophoblast. This enables the development of the conceptus in early pregnancy under low oxygen conditions, shielded from various environmental stressors. Notably, RNA-sequencing demonstrated that SUSD2⁺ stromal cells highly express genes encoding prototypic pericyte markers, including platelet-derived growth factor receptor β (*PDGFRB*), CD146 (*MCAM*), neural/glial antigen 2 (*CSPG4*), and α smooth muscle actin (*ACTA2*) [28,29]. Hence, hereafter SUSD2⁺ cells are termed perivascular cells (PVC) whereas SUSD2⁻ stromal cells are referred to as endometrial stromal cells (EnSC). On average 6% and 94% of non-immune stromal cells isolated from midluteal biopsies are PVC and EnSC, respectively. [27]

The metabolome encompasses a plethora of small organic molecules below 1.5 kDa with diverse physical and chemical structures, including nucleosides, amino acids, carbohydrates, and lipids. [30] Exometabolomics, also known as metabolic footprinting, is the study of how cells transform their surrounding microenvironment through the secretion of metabolites. Exometabolomics have been used to study the secreted metabolome profile of micro-organisms, with mammalian exometabolomics being a nascent field. [31,32] To date exometabolomics has been performed to understand differences in profile of breast cancer cell lines, T-cell immunity, and stem cells. [33-35]

In this study, we used both untargeted and targeted LC-MS exometabolomics to map the dynamic changes in the metabolic footprints of 12 paired PVC and EnSC cultures decidualized over an 8-day time-course.

## MATERIALS AND METHODS

### Endometrial tissue collection

The study was approved by the NHS National Research Ethics – Hammersmith and Queen Charlotte's & Chelsea Research Ethics Committee (1997/5065). Endometrial biopsies were obtained in the Implantation Clinic, a specialized research clinic at University Hospitals Coventry and Warwickshire National Health Service Trust. Written informed consent was given by all participants in accordance with The Declaration of Helsinki 2000. Endometrial biopsies, timed 6 to 10 days following the preovulatory luteinizing hormone surge, were taken using a Wallach EndocellTM sampler (Wallach, Trumbull, USA) following a transvaginal ultrasound scan to exclude overt uterine pathology. Further, none of the participants had been prescribed hormonal treatment in at least 3 months prior to biopsy.

### Isolation of PVC and EnSC from endometrial biopsies

Single-cell suspensions of EnSC were isolated from 12 midluteal biopsies as described previously. [36] In short, samples were collected in DMEM/F-12 with 10% dextran coated charcoal activated fetal bovine serum (DCC-FBS), finely chopped, and enzymatically digested with deoxyribonuclease type I (0.1 mg/mL; Roche, Burgess Hill, UK) and collagenase (0.5 mg/mL; Sigma-Aldrich, Gillingham, UK) for 1 h at 37°C. The cells were passed through a 40 µm cell strainer (Fisher Scientific, Loughborough, UK), which retained epithelial cells more resistant to enzymatic digestion. Ficoll-Paque PLUS (GE Healthcare, Little Chalfont, UK) was utilized to remove erythrocytes from the stromal cell fraction. Subsequently, SUSD2$^+$ and SUSD2$^-$ cells

were isolated using magnetic bead sorting, as detailed previously. [36] Briefly, up to $1 \times 10^6$ EnSC/100 µL of Magnetic Bead Buffer (0.5% BSA in PBS) were combined with 5 µL/$1 \times 10^6$ cells phycoerythrin (PE) conjugated anti-human SUSD2 antibody (BioLegend, London, UK). After 20 min on ice, approximately $1 \times 10^7$ cells/80 µL of Magnetic Bead Buffer were incubated with anti-PE-magnetic-activated cell sorting MicroBeads (20 µL/$1 \times 10^7$ cells; Miltenyi Biotec, UK) for another 20 min. Cell suspensions (up to $1 \times 10^8$ cells/500 µL of Magnetic Bead Buffer) were applied onto MS columns (Miltenyi Biotec) in a magnetic field, and washed multiple times with 500 µL of Magnetic Bead Buffer. SUSD2$^-$ cells passed freely through the column, whereas magnetically labelled SUSD2$^+$ cells were retained Following removal from the magnetic field, SUSD2$^+$ cells were eluted from the columns with 1 mL of Magnetic Bead Buffer. Purified SUSD2$^-$ and SUSD2$^+$ cells were expanded in DMEM/F12 with 10% DCC-FBS, 1% antibiotic-antimycotic solution (Invitrogen), 1% L-glutamine (Invitrogen), estradiol (1 nM; Sigma-Aldrich), insulin (2 µg/mL; Sigma-Aldrich), and basic fibroblast growth factor (10 ng/mL; Merck Millipore, Watford, UK). Decidualization experiments were carried out at passage 2. Briefly, paired SUSD2$^-$ and SUSD2$^+$ cells were seeded 6-well plates at a density of $2 \times 10^5$ cells/well and decidualized when 90% confluent with 0.5 mM 8-bromoadenosine cAMP (8-bromo-cAMP; Sigma-Aldrich) and 1 µM medroxyprogesterone acetate (MPA; Sigma-Aldrich) in phenol red-free DMEM/F12 containing 2% DCC-FBS, 1% antibiotic-antimycotic solution. The spent medium was collected every 48 h for analysis and the differentiation medium refreshed.

**Preparation of spent medium for analysis**

For untargeted exometabolome analysis, samples were prepared as described previously, [37,38] with some modifications. Briefly 50 µL of EnSC and PVC conditioned media were thawed at 4°C, and quality control (QC) samples were prepared by mixing an equal amount of conditioned media from each of the samples. Both QC and the conditioned media from PVC and EnSC were

7

processed in the same way. Proteins were precipitated with 200 µL ice-cold methanol containing 10 µg/mL 9-fluorenylmethoxycarbonyl-glycine as an internal standard (ISTD), and vortexed. Following centrifugation at 16,000 rpm for 10 min at min at 4 °C, the supernatant was collected and evaporated until dry in a speed vacuum evaporator then resuspended in 200 µL of water/methanol (98:2; v/v) for liquid chromatography-mass spectrometry (LC-MS) analysis. All samples were kept at 4°C and analyzed within 48 h. The sample run order was randomized to remove batch effects and the QC samples were analyzed after every eight samples to monitor the stability of the system.

**Untargeted LC-MS exometabolomics**

Untargeted exometabolomics was performed as previously described.[39] The prepared conditioned media was analyzed using Agilent 1290 ultrahigh-pressure liquid chromatography system (Waldbronn, Germany) equipped with a 6520 QTOF mass detector managed by a MassHunter workstation. The oven temperature was set at 45°C.

The 5 µL  of injected sample was separated using an Agilent rapid resolution HT Zorbax SB-C18 column (2.1×50 mm, 1.8 mm; Agilent Technologies, Santa Clara, CA, USA), 0.4 mL/min flow rate,  and a gradient elution involving a mobile phase consisting of (A) 0.1% formic acid in water and (B) 0.1% formic acid in methanol. To start the mobile phase was set at 5% B, with a 7-minute linear gradient to 70% B, then a 12 min gradient to 100% B. This was held for 3 minutes then returned to 5% B in 0.1 min.

Both positive and negative electrospray ionization were used to collect mass data between m/z 100 and 1000 at a rate of two scans per second. The ion spray was set at 4,000 V, and the heated capillary temperature was maintained at 350°C. The drying gas and nebulizer nitrogen gas flow rates were 12.0 L/min and 50 psi, respectively. Two reference masses (m/z 121.0509 ($C_5H_4N_4$)

and m/z 922.0098 (C18H18O6N3P3F24) were continuously infused to the system to allow constant mass correction during the run.

**Targeted LC-MS exometabolomics**

Adenosine, inosine, hypoxanthine, and xanthine were measured and analyzed. The targeted LC-MS/MS analysis was conducted as described previously with some modifications [34]. Briefly, LC-MS analysis was performed with Agilent 1290 ultrahigh-pressure liquid chromatography system (Waldbronn, Germany) coupled to an electrospray ionization with iFunnel Technology on an Agilent 6490 triple quadrupole mass spectrometer.

The auto-sampler was cooled at 4°C and 2 μL of injected sample was chromatographically separated using an Atlantis HILIC column (2.1×100 mm; Waters, Eschbornn, Germany). The mobile phases were (A) 10mM ammonium formate and 0.1% formic acid in water and (B) 0.1% formic acid in acetonitrile. Initially, 100% was utilized for 2 min, then reduced to 80% in a linear gradient for 11 min, and to 40% B over 1 min. This as held for 5 min and then the mobile phase was returned to starting conditions over 6 min. The column was kept at 45°C and the flow rate was 0.4 mL/min. Direct infusion of individual standard solutions allowed optimization of both the mass transition and collision energy for each compound by direct infusion. Both positive and negative electrospray ionization modes were performed with the following source parameters: drying gas temperature at 250°C with a flow of 14 L/min, sheath gas temperature at 400°C with a flow of 11 L/min, nebulizer gas pressure at 40 psi, capillary voltage 4,000 V and 3,500V for positive and negative mode respectively, and nozzle voltage 500 V for both positive and negative modes.

**Data analysis**

Raw spectrometric data in untargeted metabolomics were analyzed by MassHunter Qualitative Analysis software (Agilent Technologies, US). The Molecular Feature Extractor algorithm was used to obtain the molecular features, employing the retention time (RT), chromatographic peak intensity and accurate mass as input. Next, the features were analyzed by MassHunter Mass Profiler Professional software (Agilent Technologies, US). Here, only features detected in at least 80% of the samples at the same sampling time point signal with an intensity ≥20,000 counts, three-times the limit of detection of the LC-MS instrument, were kept for further processing. The tolerance window for alignment of RT and m/z values was set at 0.15 min and 2 mDa respectively, and the data normalized to the 9-fluorenylmethoxycarbonyl-glycine ISTD spike.

Raw spectrometric data in targeted metabolomics were processed using MassHunter Workstation Quantitative Analysis software (Agilent Technologies, US). Missing values were obtained using half the lowest value. For both untargeted and targeted analysis, metabolites that were differentially expressed were inputted into the Metaboanalyst Pathway Analysis Tool to identify pathways that were altered during decidualization or between PVC and EnSC. This incorporates both pathway topology and enrichment analysis to output pathways that have changed significantly, and the pathway impact [40]. The pathway impact is calculated by the number of compounds that are significantly altered in relation to the total number of compounds in the pathway. [40]

**Statistical Analysis**

For statistical analysis, nonparametric Test (Wilcoxon, Mann–Whitney test) with Holm-Sidak Multiple Testing Correction was employed and statistical significance was set at $p<0.05$. For multivariate data analysis using hierarchical clustering or partial least squares regression (PLSR) analysis, data were normalized by applying log2, median-centering and dividing by standard deviation. Hierarchical clustering unsupervised Euclidean distance hierarchical clustering was

10

performed using HemI. [41] In addition, fold change (FC) analysis was performed to further filter the features and only those features with FC >1.5 were selected as potential significantly altered metabolites across decidualization.

**Compound identification**

The identification of the differential metabolites structure was based on our published work. [39] Briefly, Masshunter software (Agilent) was used to calculate the elemental compositions of the metabolites based on their exact mass, the isotope pattern, and the nitrogen rule. The elemental composition in combination with the exact mass were used in open source database searches, including HMDB (http://www.hmdb.ca/), LIPIDMAPS (http://www.lipidmaps.org/), MassBank (http://www.massbank.jp/), and METLIN (http://metlin.scripps.edu/). Next, MS/MS experiments were performed to obtain structural information from the fragmentation pattern of the metabolite and these MS/MS spectra were searched and compared to compounds in the databases. Finally, the metabolites were confirmed by comparison with the standards where commercially available. The metabolites meet the minimum reporting standards for chemical analysis in metabolomics recommended by Metabolomics Standard Initiative (MSI). [42]

## RESULTS

### Exometabolic footprints of decidualizing primary EnSC

The endometrial stromal fraction of 12 midluteal biopsies were separated into SUSD2$^+$ PVC and SUSD2$^-$ EnSC by magnetic-activated cell sorting (MACS). Both subpopulations were cultured to confluency and then decidualized with 8-bromo-cAMP and MPA (medroxyprogesterone acetate, a progestin) over 8 days. Conditioned culture media of paired decidualizing PVC and EnSC cultures were collected every 48 h and subjected LC-MS based metabolomics (Fig. 1). A total of 145 annotated secreted metabolites and 5 unidentified metabolites were detected in the conditioned media of both PVC and EnSC (Table S1). There were no metabolites unique to either PVC or EnSC. Hence, the metabolite data of PVC and EnSC were first combined to construct a temporal map of metabolic footprints associated with decidualization.

The QC samples clustered together in principal component analysis (PCA) scores plots (Fig. S1), indicating good stability and reproducibility of the chromatographic separation throughout the entire sequence. PLSR analysis separated the decidual time points into distinct groups (Fig. 2A). Regression coefficients were used to identify metabolites that shaped the progression of decidualizing cells throughout the time-course. Metabolites with the five highest β-coefficient (β) at each timepoint are depicted in Figure 2B. Phenylalanyl-tyrosine (β: 0.02), 2,3-dinor-8-isoprostaglandin $F_{2\alpha}$ (2, 3-dinor-8-isoPGF$_{2\alpha}$) (β: 0.01), and hypoxanthine (β: 0.02) were identified, respectively, as influencers on day 0 (undifferentiated cells), day 2 and day 4 of the decidual time-course. Adenosine thiamine triphosphate (AThTP) (β: 0.01) and hyaluronic acid (β: 0.01) were the highest influencers of day 8 of decidualization.

The exometabolome analysis of conditioned media revealed a marked temporal change in metabolic footprints upon decidualization. Out of the 150 detected compounds, the secreted

12

levels of 79 metabolites changed by $\geq$1.5-fold ($p$<0.05) over the 8-day decidual time-course (Fig. 3A, Table S2). Unsupervised hierarchical clustering showed a major bifurcation in exometabolome profiles between undifferentiated and decidualizing cells. Further, each decidual time-point was characterized by a unique footprint, which supports the notion that decidualization is a multistep differentiation process (Fig. 3A).

Figure 3B highlights several regulated secreted metabolites, some of which are already implicated in decidualization. For example, the prostaglandin metabolite, 2, 3-dinor-8-isoPGF$_{2\alpha}$, which can be derived from PGE$_2$, was undetectable in undifferentiated cultures but consistently upregulated in differentiating cells throughout the decidual time-course. Secreted levels of glucosylsphingosine, a sphingolipid metabolite, followed the same pattern, in keeping with the dependency of the decidual process on *de novo* sphingolipid synthesis. [43,44] Several metabolites were selectively secreted by the decidualizing cells on day 8, including 5-amino-3-oxohexanoate and hyaluronic acid (HA). HA prevents apoptosis of decidual cells through binding to its receptor CD44. [45] 20-trihydroxy-leukotriene-B4 and PE (18:3/14:1) are examples of metabolites inhibited upon decidualization, whereas phosphatidylcholine (PC) (16:0/16:0) and lactosamine exemplify metabolites exhibiting a biphasic secreted pattern, peaking on day 2 and day 4 of decidualization, respectively.

Metaboanalyst was used to identify metabolic pathways regulated upon decidualization. [40] Twenty-one metabolic pathways were identified across the decidual time-course (Table S3). As shown in Figure 3C, prominent pathways enriched across the decidual time-course included valine, leucine, and isoleucine biosynthesis (VLIB), glycerophospholipid metabolism (GM), and phenylalanine, tyrosine, and tryptophan metabolism (PTTM). Pyrimidine metabolism (PM) was enriched on day 8 of decidualization, indicating the requirement for pyrimidines, most likely as nitrogenous bases in DNA and RNA.

**Metabolites differentially secreted by decidualizing PVC and EnSC**

The temporal changes in the metabolic footprints of decidualizing PVC and EnSC were comparable but not identical, as demonstrated PLSR analysis (Fig. S2). Notably, apart from a single metabolite (N2, N2-Dimethylguanosine), no significant differences were observed in the exometabolomes of undifferentiated PVC and EnSC. By day 2 of decidualization, however, the secreted levels of 12 annotated metabolites were significantly higher in PVC compared to EnSC and 4 were lower ($\geq$1.5 fold-change, $p$<0.05; Table S4). By day 4 and day 8 of decidualization, secreted levels of 6 and 9 metabolites, respectively, were significantly different between PVC and EnSC (Table S4). Out of a total of 32 differentially secreted, annotated metabolites, 20 were more abundantly expressed by PVC. Figure 4A shows examples of metabolites differentially secreted between PVC and EnSC at each timepoint of the decidual pathway.

To further elucidate the metabolic differences between PVC and EnSC upon decidualization, pathway enrichment analysis was performed (Fig. 4B). Interestingly, distinct metabolomic profiles emerged. The citric cycle (CC) cycle, and glycine, serine and threonine metabolism (GSTM) were enriched in PVC cells on day 2 of decidualization. Enrichment of sphingolipid metabolism (SM) arose at in PVC at day 4, whereas inositol phosphate metabolism (IPM) and the pentose phosphate metabolism (PPM) were more prominent in EnSC. Finally, on day 8, sphingolipid (SM) and purine metabolism (PuM) were enriched in PVC. Purine metabolism had the highest pathway impact and significance (Fig. 4B), suggesting a greater autocrine or paracrine requirement of purine signaling upon decidualization in PVC when compared to EnSC.

**Targeted metabolomic analysis**

The enhancement in purine metabolism prompted us to investigate their wider metabolomic network in greater depth. We developed an analytically robust  targeted mass spectrometry

14

analysis (average coefficient of variation=23.9%) to assess adenosine, inosine, hypoxanthine, and xanthine levels. Adenosine (7.8 fold-change, $p$=0.0001), inosine (1.53 fold-change, $p$<0.02) and xanthine (3.1 fold-change, $p$=0.0001) were significantly higher in PVC on day 8 of the decidual time-course in comparison to undifferentiated cells whereas uridine (0.21 fold-change, $p$<0.0001) and cytidine (0.42 fold-change, $p$=0.001) were significantly lower. Furthermore, xanthine levels were significantly lower in PVC compared to EnSC conditioned media in both undifferentiated and decidualized cultures (Fig. 5B).

## DISCUSSION

Several studies have documented the dynamic changes in the EnSC transcriptome, proteome and secretome upon decidualization, [4,46,47] but changes in secreted metabolites that may function as signaling molecules have not yet been characterized. Here, we demonstrate that decidualization of EnSC and PVC induces conspicuous metabolic footprints that are tightly regulated in a temporal fashion. For instance, HA secretion was prominent upon full decidualization (day 8) in both EnSC and PVC. This ECM macromolecule has gel properties and is typically highly expressed in rapidly expanding tissues. [48] The temporally restricted pattern of HA secretion upon decidualization, therefore, suggests a potential role in decidual expansion in early pregnancy. HA also binds CD44 expressed on extravillous trophoblast and vasculature, indicating a role in spiral artery remodeling. [45] Moreover, loss of HA secretion has been linked to miscarriage, [45] which further underscores the importance of appropriate temporospatial secretion of this ECM component in pregnancy.

Our untargeted analysis also revealed significant changes in secreted lipid metabolites upon decidualization. Phosphodimethyl-EA and PC (16:0/16:0) are present in phospholipid bilayers, act as signaling molecules, and contribute phosphoethanolamine and phosphocholine, respectively, to form sphingolipids such as sphingomyelin. [49–51] Decreasing levels of Phosphodimethyl-EA, PC (16:0/16:0) upon decidualization occurred in concert with increased secretion of glucosylsphingosine, indicating a role for extracellular sphingolipids. Enhanced sphingolipid secretion corroborates recent findings from mice demonstrating that genes encoding sphingolipid producing enzymes are upregulated upon decidualization. [44] Mice deficient of these sphingolipid synthesizing enzymes exhibit impaired decidualization, reduced implantation sites, and vascular endothelial defects that compromise trophoblast from invading the maternal vasculature. [43,44] Sphingolipids play a role in angiogenesis and promote phospholipase $A_2$

16

enzymatic activity, the enzyme required to form arachidonic acid, a precursor for prostaglandins and leukotrienes.[52,53] While 20-trihydroxyleukotriene secretion decreased upon decidualization, 2,3-dinor-8-isoPGF$_{2\alpha}$ levels were consistently elevated across the time-course, suggesting that sustained *de novo* synthesis of sphingolipids is important for decidualization, as demonstrated in mice.[44]

Exometabolomic differences were also observed between PVC and EnSC. The most notable differences occurred on day 2 of decidualization, i.e. coinciding with the initial inflammatory phase.[13] The secreted response at this time-point was also more pronounced in PVC than EnSC, in keeping with the topology of decidualization *in vivo*.[4] The PVC exometabolome on day 2 was enriched in higher energy metabolites linked to pyruvate metabolism and TCA cycle, indicative of Warburg effect or active metabolism.[54] On day 8 of the decidual time-course, the PVC exometabolome was enriched for more complex metabolites, such as sphingolipids and purines involved in signaling and structural integrity.[49,55]

Purines, along with pyrimidines, stimulate purinergic receptors, which belong to two subfamilies, the P2X and P2Y receptors (P2XR and P2YR, respectively). P2XR are plasma membrane channels that increase cytosolic $Ca^{2+}$ concentration and mediate the flux of $K^+$ and $Na^+$ upon activation.[56] P2X4R is linked to PGE$_2$ signaling.[57] P2YR are G-protein coupled receptors that modulate $Ca^{2+}$ mobilization and cAMP signaling in response to either the pyrimidines adenine and uridine, or purines. The affinity for different ligands varies between receptors; for example, P2Y2R preferentially binds UTP, whereas P2Y11R binds ATP.[58] Purines modulate cell growth, act as coenzymes, and are a source of energy whereas pyrimidines contribute to phospholipid biosynthesis, glycosylation and detoxification.[59,60] Not only do endometrial cells, and particularly epithelial cells, express purinergic receptors but placental trophoblast expresses nearly the entire

repertoire of purinergic receptors. [61–63] Thus, purine and pyrimidine nucleotides potentially act as metabolic sensors that converge on the purinergic receptors at the placental-decidual interface.

Intriguingly, purine levels correlate with the induction of stress ligands expression, such as the cell surface glycoprotein MHC class I polypeptide-related sequence A (MICA), a ligand for the natural killer group 2D receptor (NKG2D). [64] Recently, uNK cells were shown to target and eliminate senescent decidual cells through activation of NKG2D receptors, [5,15] a process that is purportedly essential to prevent chronic senescence of the placental-decidual interface in pregnancy, leading to tissue breakdown and miscarriage [15].

Targeted LC-MS demonstrated markedly lower levels of xanthine in PVC compared to EnSC, irrespective of decidualization. By contrast, decidualized PVC secreted higher levels of adenosine and inosine. Adenosine is an anti-inflammatory metabolite and stress signal,[65] and parent to inosine. Inosine, an immunomodulator, is exported from cells through nucleoside transporters when intracellular concentrations are high. [65] Extracellular inosine signals through adenosine receptors and is broken down to form the downstream metabolite hypoxanthine. Xanthine is formed during the breakdown of hypoxanthine by xanthine dehydrogenase (XDH). In keeping with our observations, *XDH* transcript levels are significantly lower in PVC compared to EnSC.[4] Lower xanthine secretion by PVC suggests that higher energy purines are important in the perivascular niche as hypoxanthine is readily available to form inosine, a paracrine signaling molecule that can be recycled back to produce upstream metabolites, such as ATP. Extracellular release of ATP can induce a pro-inflammatory state, regulate the binding activity of estrogen receptors, increase production of reactive oxygen species, and induce metalloproteinase expression. [66–68] Furthermore, ATP has been shown to promote IL-8 secretion in endometrial epithelial cells and stimulate decidualization. [69] Thus, redirecting hypoxanthine towards the upstream purines may represent a mechanism to heighten decidualization of PVC cells. Taken

together, the data suggest that a balance and switch between ATP, a mainly proinflammatory molecule, and adenosine, an anti-inflammatory factor, is required for an effective decidual response.

In summary, this study is the first to map the exometabolome changes in differentiating human EnSC and to highlight the potential of different metabolites to act as autocrine or paracrine signalling molecules as the decidual process unfolds. Although the overall temporal change in metabolic footprints was remarkably consistent between decidualizing PVC and EnSC, differential secretion of specific metabolites not only reflects metabolic differences between stromal subpopulations but also raises the possibility of spatial organisation of metabolic cues at the decidual-placental interface.

## ACKNOWLEDGEMENTS

## CONFLICT OF INTEREST STATEMENT

The authors have stated that there are no conflicts of interest with this article

## AUTHOR CONTRIBUTIONS

Conceptualization: Y.H.L.; Research: J.Z., M.D.C., E.S.L., C.L., K.M.; Resources: Y.H.L., J.J.B., Q.C.; Data analysis: S.H.: Writing S.H., Y.H.L., J.J.B; Supervision: Y.H.L, J.J.B., Q.C.

# REFERENCES

1.	Brosens JJ, Parker MG, McIndoe A, Pijnenborg R, Brosens IA. A role for menstruation in preconditioning the uterus for successful pregnancy. *American Journal of Obstetrics and Gynecology*. 2009;200(6):615.e1-615.e6. doi:10.1016/j.ajog.2008.11.037

2.	Emera D, Romero R, Wagner G. The evolution of menstruation: A new model for genetic assimilation: Explaining molecular origins of maternal responses to fetal invasiveness. *BioEssays*. 2012;34(1):26-35. doi:10.1002/bies.201100099

3.	Gellersen B, Brosens JJ. Cyclic decidualization of the human endometrium in reproductive health and failure. *Endocrine Reviews*. 2014;35(6):851-905. doi:10.1210/er.2014-1045

4.	Murakami K, Lee YH, Lucas ES, et al. Decidualization Induces a Secretome Switch in Perivascular Niche Cells of the Human Endometrium. *Endocrinology*. 2014;155(11):4542-4553. doi:10.1210/en.2014-1370

5.	Brighton PJ, Maruyama Y, Fishwick K, et al. Clearance of senescent decidual cells by uterine natural killer cells in cycling human endometrium. *eLife*. 2017;6. doi:10.7554/eLife.31274.001

6.	Berkhout RP, Lambalk CB, Huirne J, et al. High-quality human preimplantation embryos actively influence endometrial stromal cell migration. *Journal of Assisted Reproduction and Genetics*. 2018;35(4):659-667. doi:10.1007/s10815-017-1107-z

7.	Weimar CHE, Kavelaars A, Brosens JJ, et al. Endometrial Stromal Cells of Women with Recurrent Miscarriage Fail to Discriminate between High- and Low-Quality Human Embryos. Lambalk CB, ed. *PLoS ONE*. 2012;7(7):e41424. doi:10.1371/journal.pone.0041424

8.	Brosens JJ, Salker MS, Teklenburg G, et al. Uterine selection of human embryos at implantation. *Scientific Reports*. 2014;4. doi:10.1038/srep03894

9.	Macklon NS, Brosens JJ. The Human Endometrium as a Sensor of Embryo Quality1. *Biology of Reproduction*. 2014;91(4):98-99. doi:10.1095/biolreprod.114.122846

10.	Nancy P, Tagliani E, Tay CS, Asp P, Levy DE, Erlebacher A. Chemokine gene silencing in decidual stromal cells limits T cell access to the maternal-fetal interface. *Science*. 2012;336(6086):1317-1321. doi:10.1126/science.1220030

11.	Erlebacher A. Immunology of the Maternal-Fetal Interface. *Annual Review of Immunology*. 2013;31(1):387-411. doi:10.1146/annurev-immunol-032712-100003

12.	Erkenbrack EM, Maziarz JD, Griffith OW, et al. The mammalian decidual cell evolved from a cellular stress response. Hurst L, ed. *PLOS Biology*. 2018;16(8):e2005594. doi:10.1371/journal.pbio.2005594

13.	Stadtmauer DJ, Wagner GP. Cooperative inflammation: The recruitment of inflammatory signaling in marsupial and eutherian pregnancy. *Journal of Reproductive Immunology*. 2020;137:102626. doi:10.1016/j.jri.2019.102626

21

14.     Al-Sabbagh M, Fusi L, Higham J, et al. NADPH Oxidase-Derived Reactive Oxygen Species Mediate Decidualization of Human Endometrial Stromal Cells in Response to Cyclic AMP Signaling. *Endocrinology*. 2011;152(2):730-740. doi:10.1210/en.2010-0899

15.     Lucas ES, Vrljicak P, Muter J, et al. Recurrent pregnancy loss is associated with a pro-senescent decidual response during the peri-implantation window. *Communications Biology*. 2020;3(1):1-14. doi:10.1038/s42003-020-0763-1

16.     Salker MS, Nautiyal J, Steel JH, et al. Disordered IL-33/ST2 Activation in Decidualizing Stromal Cells Prolongs Uterine Receptivity in Women with Recurrent Pregnancy Loss. Fritz JH, ed. *PLoS ONE*. 2012;7(12):e52252. doi:10.1371/journal.pone.0052252

17.     Vrljicak P, Lucas ES, Lansdowne L, et al. Analysis of chromatin accessibility in decidualizing human endometrial stromal cells. *FASEB Journal*. 2018;32(5):2467-2477. doi:10.1096/fj.201701098R

18.     Leitao B, Jones MC, Fusi L, et al. Silencing of the JNK pathway maintains progesterone receptor activity in decidualizing human endometrial stromal cells exposed to oxidative stress signals. *The FASEB Journal*. 2010;24(5):1541-1551. doi:10.1096/fj.09-149153

19.     Muter J, Brighton PJ, Lucas ES, et al. Progesterone-Dependent Induction of Phospholipase C-Related Catalytically Inactive Protein 1 (PRIP-1) in Decidualizing Human Endometrial Stromal Cells. *Endocrinology*. 2016;157(7):2883-2893. doi:10.1210/en.2015-1914

20.     Muter J, Alam MT, Vrljicak P, et al. The Glycosyltransferase EOGT Regulates Adropin Expression in Decidualizing Human Endometrium. *Endocrinology*. 2018;159(2):994-1004. doi:10.1210/en.2017-03064

21.     Cloke B, Huhtinen K, Fusi L, et al. The androgen and progesterone receptors regulate distinct gene networks and cellular functions in decidualizing endometrium. *Endocrinology*. 2008;149(9):4462-4474. doi:10.1210/en.2008-0356

22.     Takano M, Lu Z, Goto T, et al. Transcriptional cross talk between the forkhead transcription factor forkhead box O1A and the progesterone receptor coordinates cell cycle regulation and differentiation in human endometrial stromal cells. *Molecular Endocrinology*. 2007;21(10):2334-2349. doi:10.1210/me.2007-0058

23.     Mazur EC, Vasquez YM, Li X, et al. Progesterone receptor transcriptome and cistrome in decidualized human endometrial stromal cells. *Endocrinology*. 2015;156(6):2239-2253. doi:10.1210/en.2014-1566

24.     Kuroda K, Venkatakrishnan R, Salker MS, et al. Induction of 11β-HSD 1 and activation of distinct mineralocorticoid receptor- and glucocorticoid receptor-dependent gene networks in decidualizing human endometrial stromal cells. *Molecular Endocrinology*. 2013;27(2):192-202. doi:10.1210/me.2012-1247

25.     Kajihara T, Jones M, Fusi L, et al. Differential Expression of FOXO1 and FOXO3a Confers Resistance to Oxidative Cell Death upon Endometrial Decidualization. *Molecular Endocrinology*. 2006;20(10):2444-2455. doi:10.1210/me.2006-0118

26.     Teklenburg G, Salker M, Molokhia M, et al. Natural Selection of Human Embryos: Decidualizing Endometrial Stromal Cells Serve as Sensors of Embryo Quality upon

Implantation. Vitzthum VJ, ed. *PLoS ONE*. 2010;5(4):e10258.
doi:10.1371/journal.pone.0010258

27. Lucas ES, Dyer NP, Murakami K, et al. Loss of Endometrial Plasticity in Recurrent Pregnancy Loss. *Stem Cells*. 2016;34(2):346-356. doi:10.1002/stem.2222

28. Ferland-McCollough D, Slater S, Richard J, Reni C, Mangialardi G. Pericytes, an overlooked player in vascular pathobiology. *Pharmacology and Therapeutics*. 2017;171:30-42. doi:10.1016/j.pharmthera.2016.11.008

29. Armulik A, Genové G, Betsholtz C. Pericytes: Developmental, Physiological, and Pathological Perspectives, Problems, and Promises. *Developmental Cell*. 2011;21(2):193-215. doi:10.1016/j.devcel.2011.07.001

30. Cui L, Lu H, Lee YH. Challenges and emergent solutions for LC-MS/MS based untargeted metabolomics in diseases. *Mass Spectrometry Reviews*. 2018;37(6):772-792. doi:10.1002/mas.21562

31. Birkenstock T, Liebeke M, Winstel V, et al. Exometabolome analysis identifies pyruvate dehydrogenase as a target for the antibiotic triphenylbismuthdichloride in multiresistant bacterial pathogens. *Journal of Biological Chemistry*. 2012;287(4):2887-2895. doi:10.1074/jbc.M111.288894

32. Su Q, Guan T, Lv H. Siderophore biosynthesis coordinately modulated the virulence-associated interactive metabolome of uropathogenic Escherichia coli and human urine. *Scientific Reports*. 2016;6. doi:10.1038/srep24099

33. Ferreiro-Vera C, Mata-Granados JM, Priego-Capote F, Quesada-Gómez JM, Luque De Castro MD. Automated targeting analysis of eicosanoid inflammation biomarkers in human serum and in the exometabolome of stem cells by SPE-LC-MS/MS. *Analytical and Bioanalytical Chemistry*. 2011;399(3):1093-1103. doi:10.1007/s00216-010-4400-6

34. Garcia-Manteiga JM, Mari S, Godejohann M, et al. Metabolomics of B to plasma cell differentiation. *Journal of Proteome Research*. 2011;10(9):4165-4176. doi:10.1021/pr200328f

35. Matta P, Sherrod SD, Marasco CC, Moore DJ, McLean JA, Weitkamp J-H. In Utero Exposure to Histological Chorioamnionitis Primes the Exometabolomic Profiles of Preterm CD4 + T Lymphocytes . *The Journal of Immunology*. 2017;199(9):3074-3085. doi:10.4049/jimmunol.1601880

36. Masuda H, Anwar SS, Bühring HJ, Rao JR, Gargett CE. A novel marker of human endometrial mesenchymal stem-like cells. *Cell Transplantation*. 2012;21(10):2201-2214. doi:10.3727/096368911X637362

37. Cui L, Lee YH, Kumar Y, et al. Serum Metabolome and Lipidome Changes in Adult Patients with Primary Dengue Infection. *PLoS Neglected Tropical Diseases*. 2013;7(8). doi:10.1371/journal.pntd.0002373

38. Zhu W, Stevens AP, Dettmer K, et al. Quantitative profiling of tryptophan metabolites in serum, urine, and cell culture supernatants by liquid chromatography-tandem mass

spectrometry. *Analytical and Bioanalytical Chemistry*. 2011;401(10):3249-3261. doi:10.1007/s00216-011-5436-y

39.      Cui L, Fang J, Ooi EE, Lee YH. Serial Metabolome Changes in a Prospective Cohort of Subjects with Influenza Viral Infection and Comparison with Dengue Fever. *Journal of Proteome Research*. 2017;16(7):2614-2622. doi:10.1021/acs.jproteome.7b00173

40.      Chong J, Wishart DS, Xia J. Using MetaboAnalyst 4.0 for Comprehensive and Integrative Metabolomics Data Analysis. *Current Protocols in Bioinformatics*. 2019;68(1). doi:10.1002/cpbi.86

41.      Deng W, Wang Y, Liu Z, Cheng H, Xue Y. HemI: A Toolkit for Illustrating Heatmaps. Zhang Z, ed. *PLoS ONE*. 2014;9(11):e111988. doi:10.1371/journal.pone.0111988

42.      Sumner LW, Amberg A, Barrett D, et al. Proposed minimum reporting standards for chemical analysis: Chemical Analysis Working Group (CAWG) Metabolomics Standards Initiative (MSI). *Metabolomics*. 2007;3(3):211-221. doi:10.1007/s11306-007-0082-2

43.      Mizugishi K, Li C, Olivera A, et al. Maternal disturbance in activated sphingolipid metabolism causes pregnancy loss in mice. *Journal of Clinical Investigation*. 2007;117(10):2993-3006. doi:10.1172/JCI30674

44.      Ding NZ, Qi QR, Gu XW, Zuo RJ, Liu J, Yang ZM. De novo synthesis of sphingolipids is essential for decidualization in mice. *Theriogenology*. 2018;106:227-236. doi:10.1016/j.theriogenology.2017.09.036

45.      Takizawa T, Takahashi H, Takizawa T, et al. Extravillous trophoblast cell invasion is promoted by the CD44-hyaluronic acid interaction. *Placenta*. 2014;35(3):163-170. doi:10.1016/j.placenta.2013.12.009

46.      Garrido-Gomez T, Dominguez F, Lopez JA, et al. Modeling Human Endometrial Decidualization from the Interaction between Proteome and Secretome. *Journal of Clinical Endocrinology and Metabolism*. 2011;96(3):706-716. doi:10.1210/jc.2010-1825

47.      Rytkönen KT, Erkenbrack EM, Poutanen M, Elo LL, Pavlicev M, Wagner GP. Decidualization of Human Endometrial Stromal Fibroblasts is a Multiphasic Process Involving Distinct Transcriptional Programs. *Reproductive Sciences*. 2019;26(3):323-336. doi:10.1177/1933719118802056

48.      Karousou E, Misra S, Ghatak S, et al. Roles and targeting of the HAS/hyaluronan/CD44 molecular system in cancer. *Matrix Biology*. 2017;59:3-22. doi:10.1016/j.matbio.2016.10.001

49.      Merrill AH. Sphingolipid and glycosphingolipid metabolic pathways in the era of sphingolipidomics. *Chemical Reviews*. 2011;111(10):6387-6422. doi:10.1021/cr2002917

50.      Gault CR, Obeid LM, Hannun YA. An overview of sphingolipid metabolism: From synthesis to breakdown. *Advances in Experimental Medicine and Biology*. 2010;688:1-23. doi:10.1007/978-1-4419-6741-1_1

51.      Furse S, de Kroon AIPM. Phosphatidylcholines functions beyond that of a membrane brick. *Molecular Membrane Biology*. 2015;32(4):117-119. doi:10.3109/09687688.2015.1066894

52.     Murakami M, Kudo I. Phospholipase A2. *Journal of Biochemistry*. 2002;131(3):285-292. doi:10.1093/oxfordjournals.jbchem.a003101

53.     Singh DK, Subbaiah P v. Modulation of the activity and arachidonic acid selectivity of group X secretory phospholipase A2 by sphingolipids. *Journal of Lipid Research*. 2007;48(3):683-692. doi:10.1194/jlr.M600421-JLR200

54.     DeBerardinis RJ, Chandel NS. We need to talk about the Warburg effect. *Nature Metabolism*. 2020;2(2):127-129. doi:10.1038/s42255-020-0172-2

55.     Linden J, Koch-Nolte F, Dahl G. Purine Release, Metabolism, and Signaling in the Inflammatory Response. *Annual Review of Immunology*. 2019;37(1):325-347. doi:10.1146/annurev-immunol-051116-052406

56.     di Virgilio F, Adinolfi E. Extracellular purines, purinergic receptors and tumor growth. *Oncogene*. 2017;36(3):293-303. doi:10.1038/onc.2016.206

57.     Ulmann L, Hirbec H, Rassendren F. P2X4 receptors mediate PGE2 release by tissue-resident macrophages and initiate inflammatory pain. *EMBO Journal*. 2010;29(14):2290-2300. doi:10.1038/emboj.2010.126

58.     Giuliani AL, Sarti AC, di Virgilio F. Extracellular nucleotides and nucleosides as signalling molecules. *Immunology Letters*. 2019;205:16-24. doi:10.1016/j.imlet.2018.11.006

59.     Löffler M, Fairbanks LD, Zameitat E, Marinaki AM, Simmonds HA. Pyrimidine pathways in health and disease. *Trends in Molecular Medicine*. 2005;11(9):430-437. doi:10.1016/j.molmed.2005.07.003

60.     Yin J, Ren W, Huang X, Deng J, Li T, Yin Y. Potential Mechanisms Connecting Purine Metabolism and Cancer Therapy. *Frontiers in immunology*. 2018;9:1697. doi:10.3389/fimmu.2018.01697

61.     Roberts VHJ, Greenwood SL, Elliott AC, Sibley CP, Waters LH. Purinergic receptors in human placenta: evidence for functionally active P2X4 , P2X7, P2Y2 , and P2Y6. *American Journal of Physiology-Regulatory, Integrative and Comparative Physiology*. 2006;290(5):R1374-R1386. doi:10.1152/ajpregu.00612.2005

62.     Roberts VHJ, Waters LH, Powell T. Purinergic Receptor Expression and Activation in First Trimester and Term Human Placenta. *Placenta*. 2007;28(4):339-347. doi:10.1016/j.placenta.2006.04.007

63.     Burnstock G. Purinergic signalling in the reproductive system in health and disease. *Purinergic Signalling*. 2014;10(1):157-187. doi:10.1007/s11302-013-9399-7

64.     McCarthy MT, Moncayo G, Hiron TK, et al. Purine nucleotide metabolism regulates expression of the human immune ligand MICA. *Journal of Biological Chemistry*. 2018;293(11):3913-3924. doi:10.1074/jbc.M117.809459

65.     Kaster MP, Budni J, Gazal M, Cunha MP, Santos ARS, Rodrigues ALS. The antidepressant-like effect of inosine in the FST is associated with both adenosine A1 and A2A receptors. *Purinergic Signalling*. 2013;9(3):481-486. doi:10.1007/s11302-013-9361-8

66.     Cekic C, Linden J. Purinergic regulation of the immune system. *Nature Reviews Immunology*. 2016;16(3):177-192. doi:10.1038/nri.2016.4

67.     Chang S-J, Wang T-Y, Lee Y-H, Tai C-J. Extracellular ATP activates nuclear translocation of ERK1/2 leading to the induction of matrix metalloproteinases expression in human endometrial stromal cells. *Journal of Endocrinology*. 2007;193(3):393-404. doi:10.1677/JOE-06-0168

68.     Cruz CM, Rinna A, Forman HJ, Ventura ALM, Persechini PM, Ojcius DM. ATP activates a reactive oxygen species-dependent oxidative stress response and secretion of proinflammatory cytokines in macrophages. *Journal of Biological Chemistry*. 2007;282(5):2871-2879. doi:10.1074/jbc.M608083200

69.     Gu XW, Yang Y, Li T, et al. ATP mediates the interaction between human blastocyst and endometrium. *Cell Proliferation*. 2020;53(2). doi:10.1111/cpr.12737

**FIGURE LEGENDS**

**Figure 1:** Schematic representation of experimental design and the analytical process. Paired PVC and EnSC cultured were established from 12 endometrial biopsies. Conditioned media was collected from undifferentiated cultures (D0, day 0) and after 2, 4, and 8 days of decidualization.
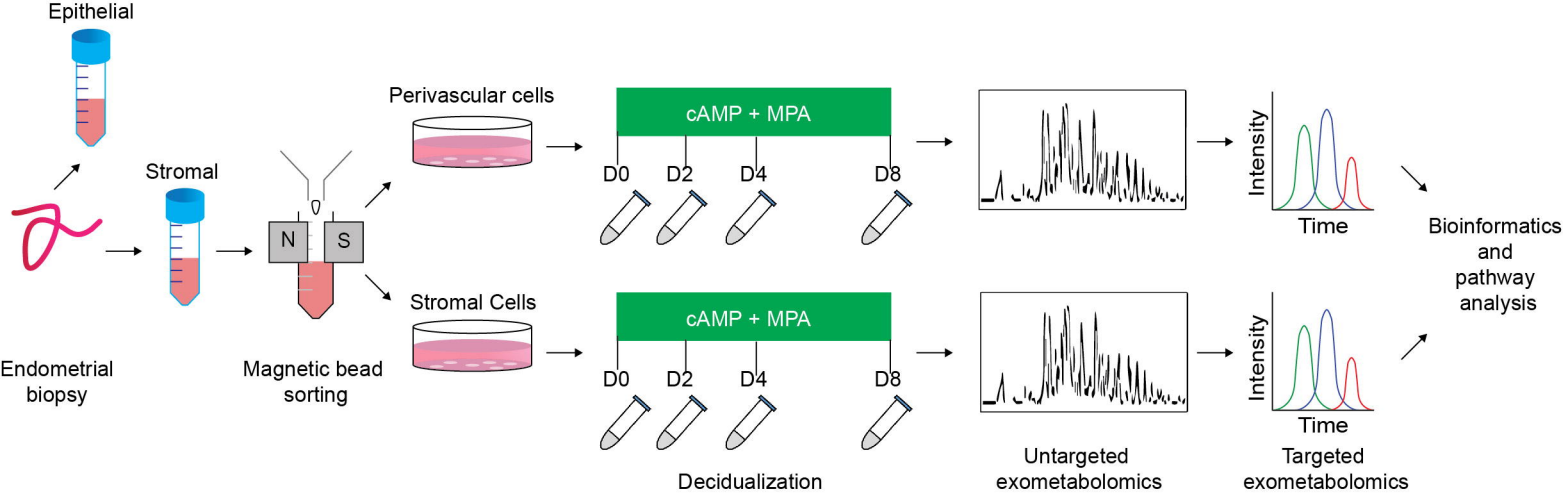
**Figure 2:** Temporal exometabolome of EnSC. A) Partial least squares regression (PLSR) analysis separated the exometabolomes according to decidual time-points. The secreted metabolite levels were log2 transformed, the data centred using median, and scaled by SD. B) Metabolites with the top five PLSR regression coefficients across the decidual time-course.
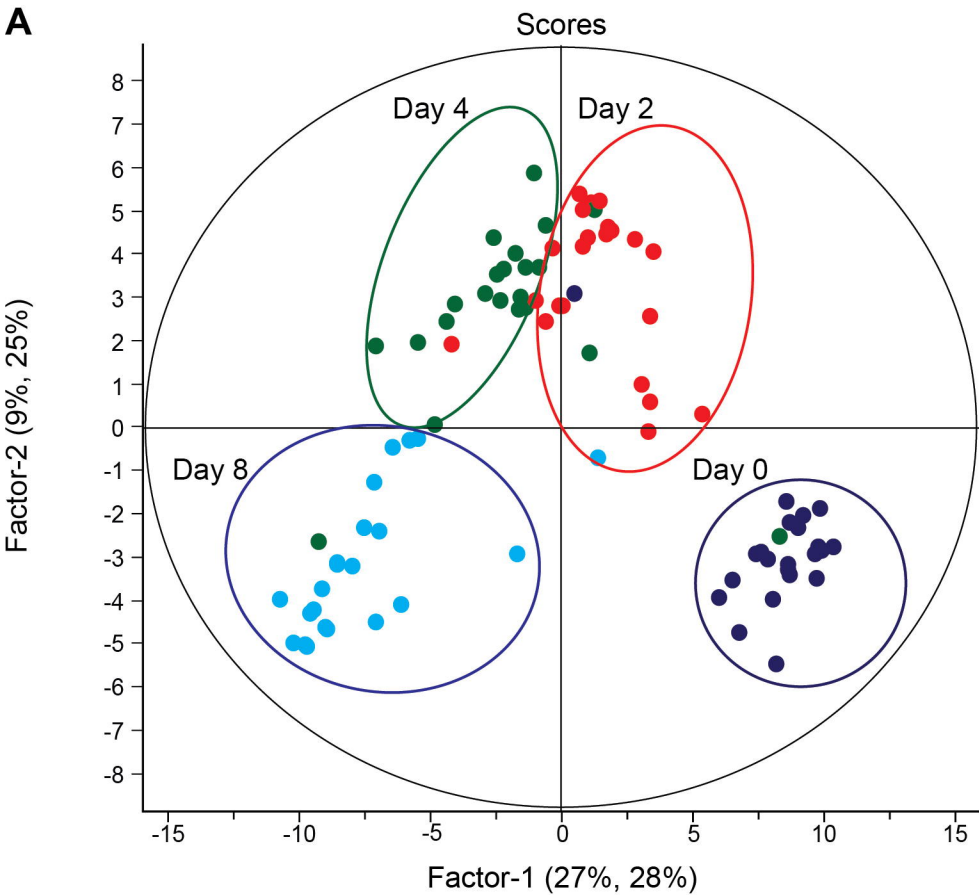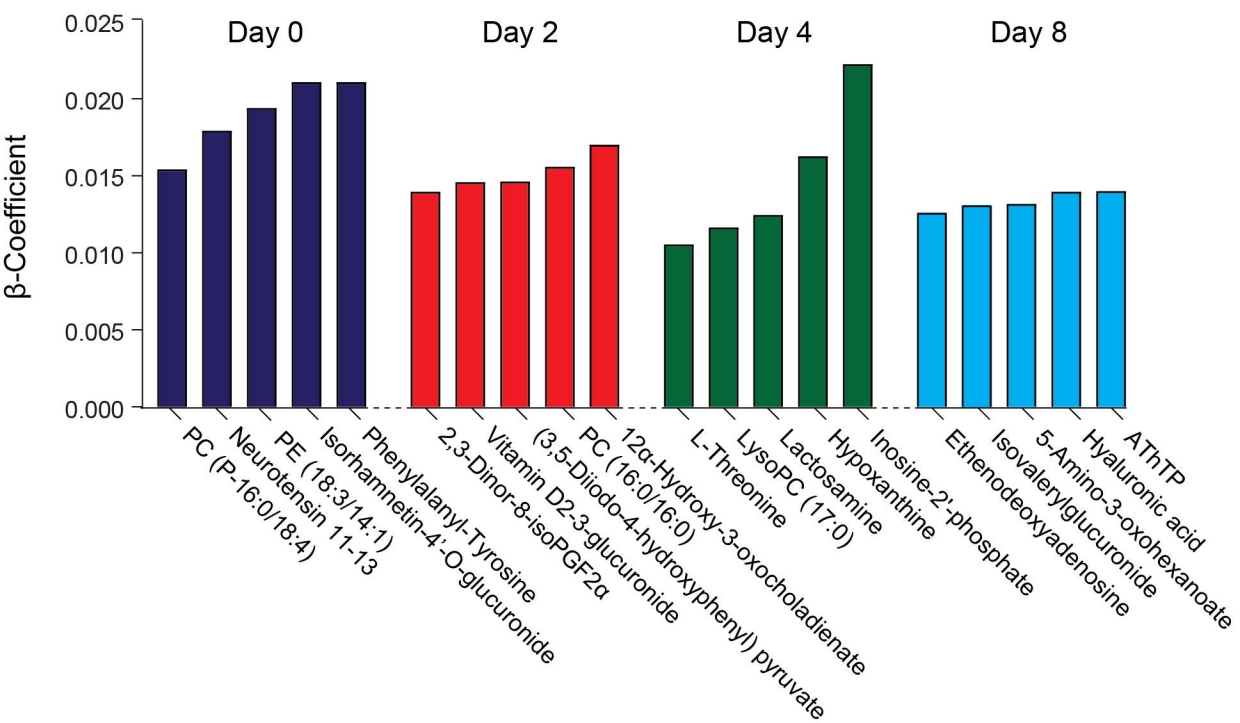
**Figure 3:** Exometabolic footprints of decidualizing primary EnSC. A) Heatmap of differentially secreted metabolites across the time-course based on unsupervised Euclidean distance hierarchical clustering. (B) Representative metabolites altered upon decidualization. Data represent mean ± SD. N.D, not detected. Different letters above the SD indicates differential secretion at the indicated time-point ($p<0.05$; $t$-test with Holm-Sidak correction). C) MetaboAnalyst pathway analysis across decidualization in EnSC. Enriched pathways include valine, leucine, and isoleucine biosynthesis (VLIB); glycero-phospholipid metabolism (GM);
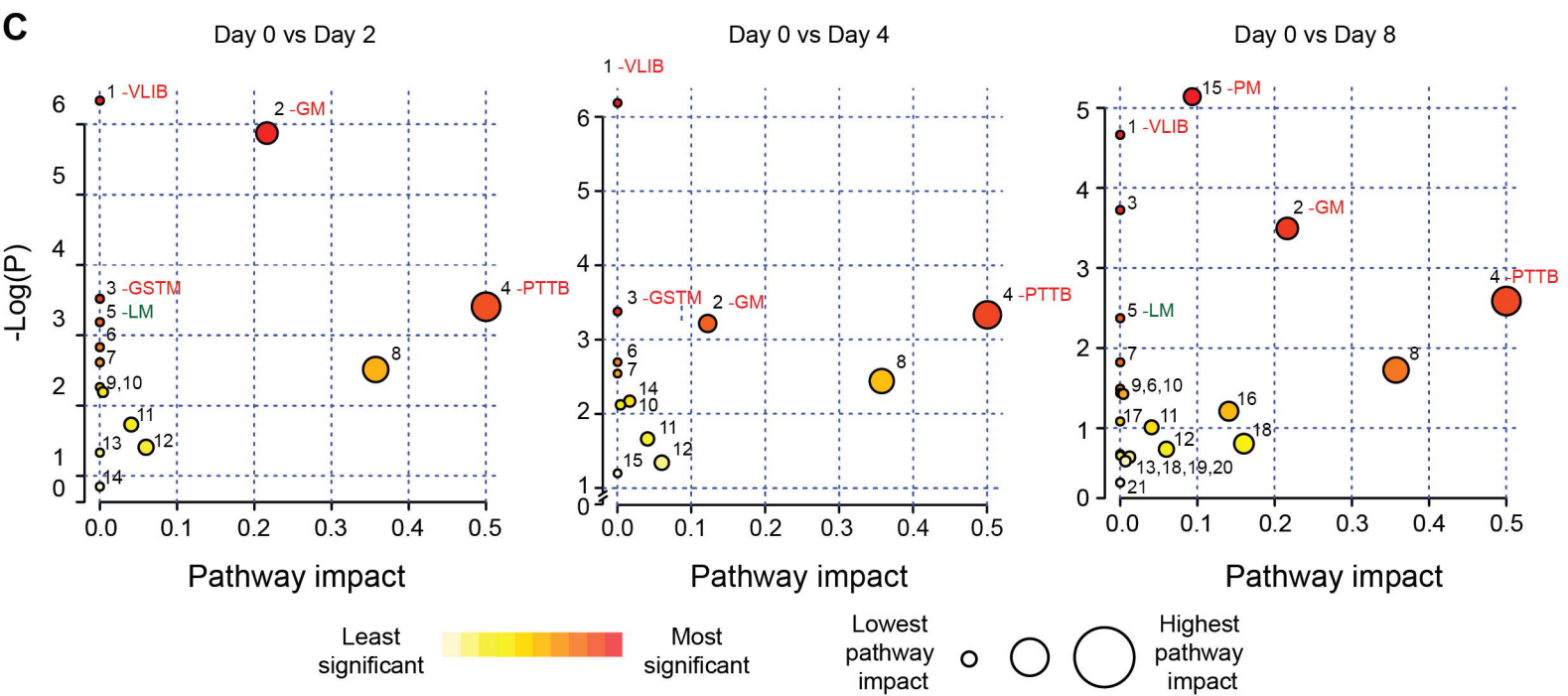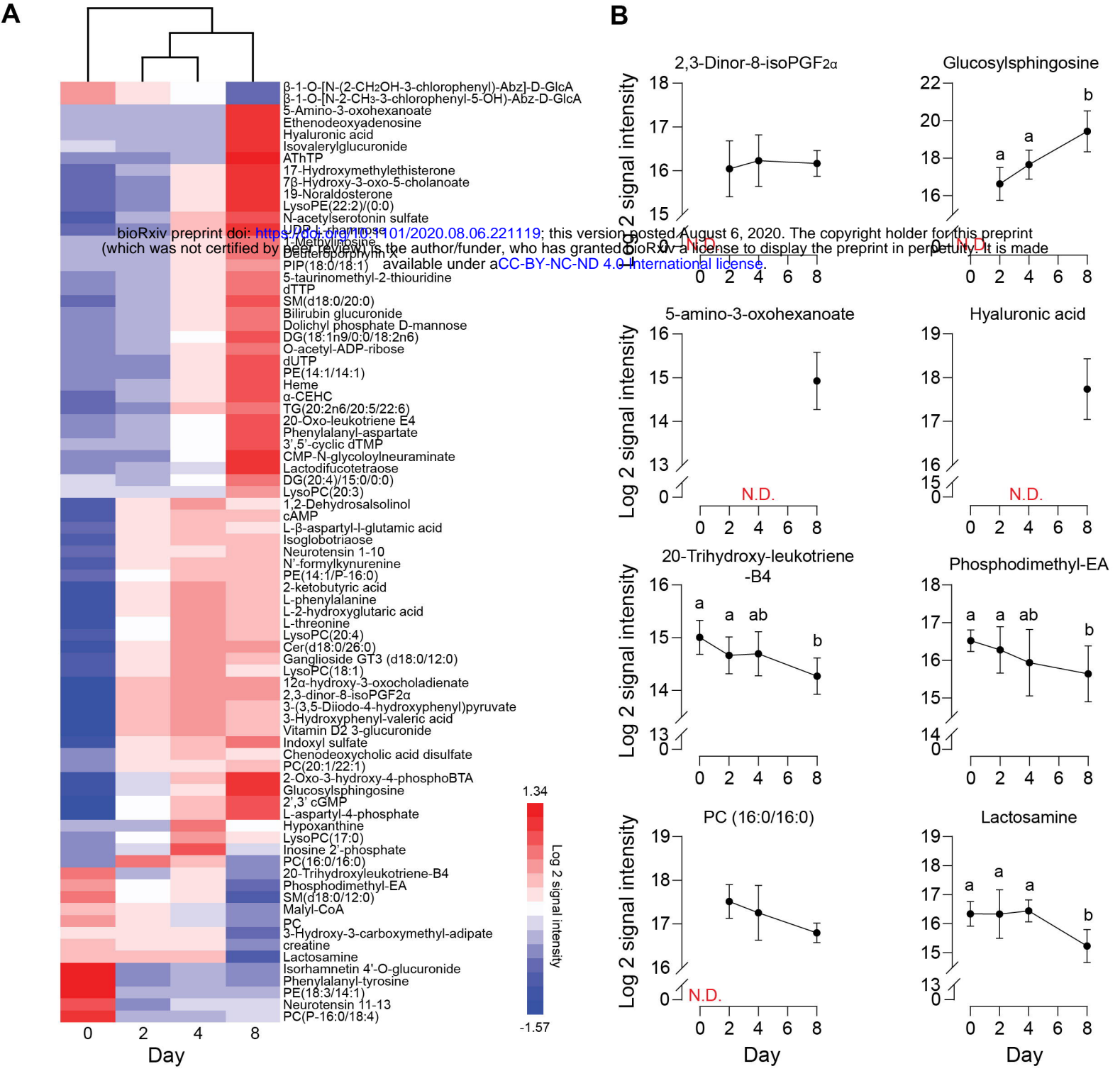
glycine, serine, and threonine metabolism (GSTM); Phenylalanine tyrosine and tryptophan biosynthesis (PTTB); Linoleic acid metabolism (LM); and pyrimidine metabolism (PM). Other pathways are tabulated in Supplementary Table 3.
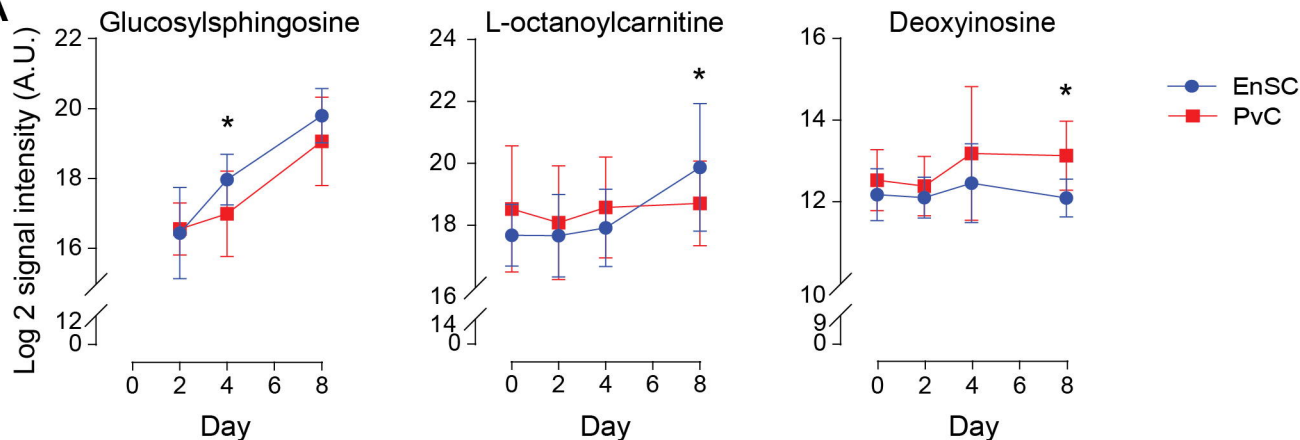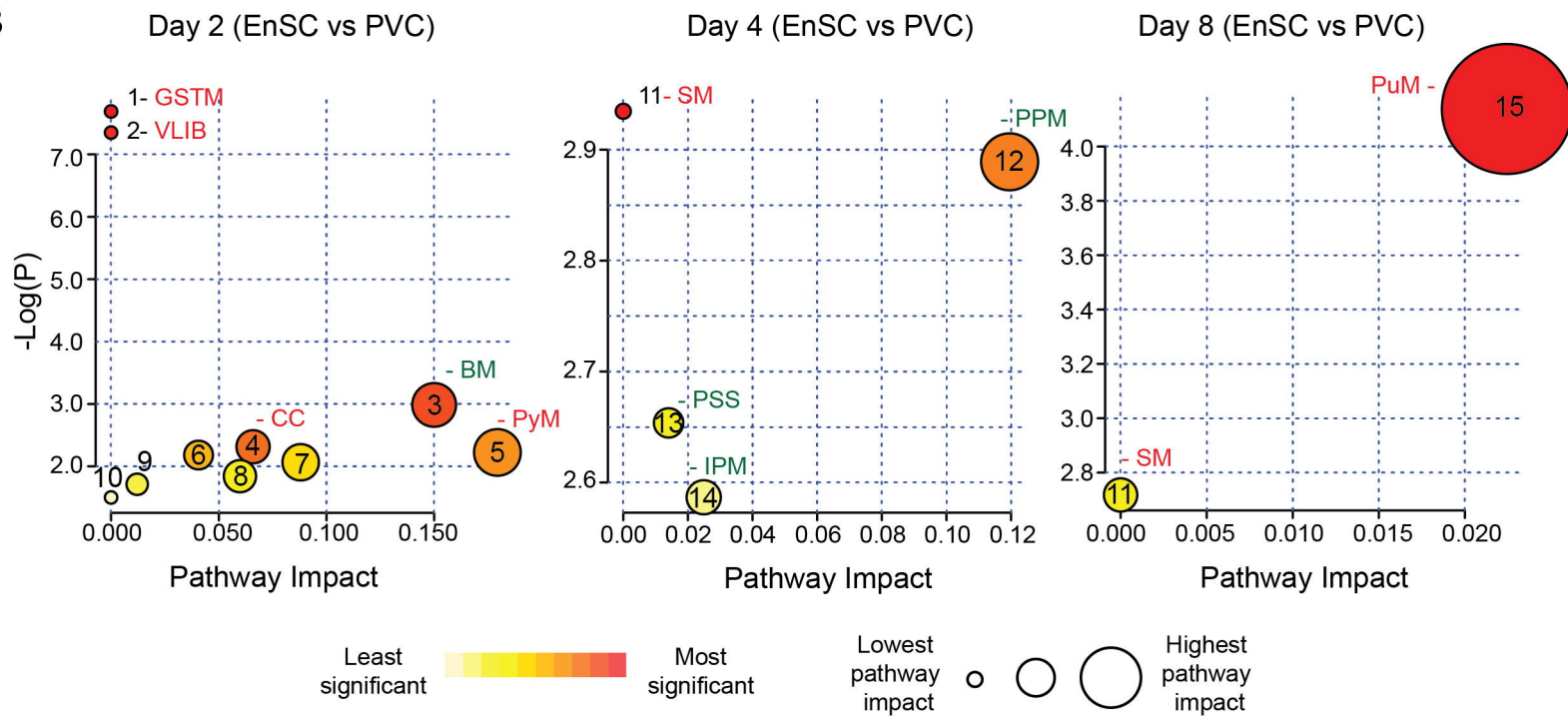
**Figure 4:** Metabolites differentially secreted by decidualizing PVC and EnSC. Data represents mean ± SD. * indicates $p<0.05$ (*t*-test with Holm-Sidak correction). B) Metaboanalyst Pathway analysis comparing PVC to EnSC of untargeted metabolomics by for day two, four and eight decidualization. Pathways labelled: glycine, serine, and threonine metabolism (GSTM), valine, leucine, and isoleucine biosynthesis (VLIB), biotin metabolism (BM), citrate cycle (CC), pyruvate metabolism (PyM), sphingolipid metabolism (SM), pentose phosphate metabolism (PPM), phosphatidylinositol signalling system (PSS), inositol phosphate metabolism (IPM) and purine metabolism (PuM). Other pathways can be found in Supplementary Table 5.

**Figure 5:** Targeted metabolomic analysis. A) Schematic overview of the purine metabolic pathway. B) Secreted purine metabolites were measured by targeted mass spectrometry in conditioned medium of paired PVC and EnSC cultures decidualized for 8 days. The data show the relative change in secreted metabolite levels in PVC compared to EnSC cultures. The data are mean ± SD and the individual data points show variability between paired cultures. * indicates $p<0.05$ (*t*-test with Holm-Sidak correction).

Epithelial

Stromal

Endometrial biopsy

Magnetic bead sorting

N   S

Perivascular cells

cAMP + MPA

D0   D2   D4   D8

Stromal Cells

cAMP + MPA

D0   D2   D4   D8

Decidualization

Untargeted exometabolomics

Intensity

Time

Targeted exometabolomics

Intensity

Time

Bioinformatics and pathway analysis

**A**

Scores

Factor-2 (9%, 25%) *(y-axis)*

Factor-1 (27%, 28%) *(x-axis)*

Day 4
Day 2
Day 8
Day 0

**B**

β-Coefficient *(y-axis)*

Day 0  Day 2  Day 4  Day 8

PC (P-16:0/18:4)
Neurotensin 11-13
PE (18:3/14:1)
Isorhamnetin-4'-O-glucuronide
Phenylalanyl-Tyrosine
2,3-Dinor-8-isoPGF2α
Vitamin D2-3-glucuronide
(3,5-Diiodo-4-hydroxyphenyl) pyruvate
PC (16:0/16:0)
12α-Hydroxy-3-oxocholadienate
L-Threonine
LysoPC (17:0)
Lactosamine
Hypoxanthine
Inosine-2'-phosphate
Ethenodeoxyadenosine
Isovalerylglucuronide
5-Amino-3-oxohexanoate
Hyaluronic acid
AThTP

A



B

**A**

Adenine → AMP

AICAR → IMP

ATP ⇌ ADP ⇌ AMP ← IMP

AMP ⇅ Adenosine (ADK)

Adenosine → Inosine (ADA)

IMP → Inosine

Inosine → Hypoxanthine (PNP)

Hypoxanthine → Xanthine (XDH)

Xanthine → Uric acid (XDH)

HPRT1

**B**

Adenosine *

Inosine *

Hypoxanthine

Xanthine *